https://doi.org/10.5194/egusphere-2026-1033
Preprint. Discussion started: 2 April 2026

A hybrid model based on Boruta feature selection and neural network for forecasting hydrological drought

Min Li[1], Yuhang Yao[1], Ming Ou[1], Changman Yin[1]

[1]College of Hydraulic Science and Engineering, Yangzhou University, Yangzhou, China, 225000

Correspondence to: Min Li (limintju@126.com)

Abstract: Accurate hydrological drought prediction is vital for water management. This study proposes a hybrid model combining Boruta feature selection, convolutional neural network (CNN), and bidirectional long short-term memory (BiLSTM) methods, to predict hydrological drought in the Huaihe River Basin of China. The Boruta algorithm selected key predictors from 31 potential drought-influencing factors. By comparing the established model Boruta-CNN-BiLSTM with other models, including Boruta-CNN-LSTM, Boruta-CNN-XGBoost, Boruta-BiLSTM, Boruta-LSTM, and Boruta-XGBoost, the results show Boruta significantly enhances all models. The Boruta-CNN-BiLSTM model has achieved the highest accuracy across 28 basin grid regions, exhibiting the largest performance gains. Furthermore, the prediction performance of the model is mainly influenced by factors such as precipitation, volumetric soil water (0-7cm), volumetric soil water (7-28cm) and surface net solar radiation. The model's prediction performance is most affected by precipitation, followed by volumetric soil water (0-7cm), volumetric soil water (7-28cm), and surface net solar radiation has the least impact. It provides enhanced support for basin-scale drought risk assessment and water resources management.

Keywords: Drought forecasting; hybrid machine learning; Boruta; SRI; Huaihe River Basin

1 Introduction

Drought is one of the most widespread natural disasters globally, causing significant economic losses (Apurv et al., 2017; Dikshit and Pradhan, 2021; Zhou et al., 2021; Li et al., 2024). In recent years, the frequency of drought events has increased due to global warming in the climate, posing severe threats to food production and water resource management (Zhang et al., 2019; Zhang et al., 2022; Wang et al., 2022). Therefore, the development of accurate drought prediction models is crucial for enhancing drought resilience, effectively managing water resources, and reducing drought-related losses.

https://doi.org/10.5194/egusphere-2026-1033
Preprint. Discussion started: 2 April 2026

However, the complex nature of droughts and their variability across different regions make monitoring and predicting droughts inherently challenging. To address these challenges, researchers have developed various drought indices, such as the Palmer Drought Severity Index (PDSI) (Palmer, 1965), the Standardized Precipitation Index (SPI) (McKee et al., 1993), and the Standardized Runoff Index (SRI) (Shukla and Wood, 2008). Each drought index has its unique advantages and limitations. The SRI index has been widely adopted in many studies to characterize hydrological droughts (Li et al., 2019; Kubiak-Wójcicka and Juskiewicz, 2020; Kadapala et al., 2024; Liu et al., 2024a). Because it provides a reliable measure of drought severity based on runoff data and is easy to calculate, versatile, and capable of assessing droughts over multiple time scales (Achite et al., 2023). Hence, this study employs the SRI to characterize hydrological droughts.

In recent years, machine learning has been very popular in the field of drought prediction (Sun and Scanlon, 2019; Ardabili et al., 2020; Zounemat-Kermani et al., 2021; Gyaneshwar et al., 2023). Numerous studies have shown that models such as Support Vector Machines (SVM), Random Forests (RF), Convolutional Neural Networks (CNN), and Long Short-Term Memory Networks (LSTM) perform strongly in predicting drought events, particularly when dealing with complex, nonlinear data (Chen et al., 2024; Elbeltagi et al., 2023; Khan et al., 2020; Kheyruri et al., 2023; Kuswanto and Naufal, 2019; Liu et al., 2024b; Zhu et al., 2021). However, single models often fail to perform well in many complex hydrological situations. To overcome these limitations, existing hybrid models attempt to combine the strengths of multiple models. For instance, Wu et al. (2022) demonstrated that integrating atmospheric circulation models with a dynamic LSTM hybrid model can significantly improve seasonal drought prediction accuracy in China. Similarly, Xu et al. (2022) employed an ARIMA-LSTM hybrid model to enhance drought prediction capabilities based on the Standardized Precipitation Evapotranspiration Index (SPEI). Yalcin et al. (2023) utilized a model combining CNN and LSTM, which exhibited significant advantages in the time series prediction of drought indices, particularly in processing complex time series data, thereby improving spatiotemporal consistency and prediction accuracy. While these hybrid models have achieved significant advancements by leveraging the strengths of multiple models, they still face major challenges in feature selection. Poor feature selection can lead to unstable model performance and increased computational costs, limiting the overall effectiveness of these approaches (Karbasi et al., 2024). Therefore, it is necessary to explore optimized feature selection

https://doi.org/10.5194/egusphere-2026-1033
Preprint. Discussion started: 2 April 2026

methods to enhance the stability and accuracy of these models when applied to complex drought prediction scenarios.

Given the importance of feature selection, optimizing this aspect is crucial for improving the performance of machine-learning models in drought prediction (Li et al., 2017; Prodhan et al., 2022; Nandgude et al., 2023). Previous studies have demonstrated that advanced feature selection techniques can significantly enhance model performance. For example, Karbasi et al. (2024) utilized the Boruta feature selection algorithm for feature selection and combined it with a Bidirectional Long Short-Term Memory Network (BiLSTM), which significantly improved the performance of the model in pan evaporation forecasting, especially under complex climatic conditions, achieving higher predictive accuracy. Sayyad et al. (2022) showed that a hybrid feature selection method combining Random Forest and Principal Component Analysis (PCA) can effectively reduce feature redundancy, thereby enhancing model accuracy and robustness in tool wear prediction. Ahmed et al. (2021) combined a feature extraction algorithm based on the Boruta-Random Forest approach with an LSTM model to predict river water levels, which effectively improved the predictive performance of the model. As a powerful feature selection method, the Boruta-random forest hybridizer algorithm is particularly noteworthy. It can identify the features that are most relevant to the target variable and eliminate unnecessary features (Kursa et al., 2010; Christ et al., 2017; Prasad et al., 2019; Subbiah et al., 2023). These selected features are then used as inputs to various nonlinear models. By integrating feature selection with advanced machine learning techniques, the overall predictive performance can be significantly enhanced.

Most existing models still have significant limitations in feature selection, failing to fully consider multidimensional data characteristics in complex hydrological environments, resulting in unstable performance when dealing with highly nonlinear data. Furthermore, although hybrid models have attempted to combine the advantages of multiple algorithms, they still lack in optimizing the matching between input features and model structures, leading to limitations in prediction accuracy. Based on these shortcomings, the primary objective of this study is to develop a novel hybrid machine learning model, the Boruta-CNN-BiLSTM model, to improve the accuracy of hydrological drought prediction. First, the study aims to accurately select features most relevant to hydrological droughts using the Boruta-random forest hybridizer algorithm, thereby reducing feature redundancy and mitigating the overfitting risk. Second, these selected features will be combined with the CNN-BiLSTM model to fully leverage the

https://doi.org/10.5194/egusphere-2026-1033
Preprint. Discussion started: 2 April 2026

spatial feature extraction capabilities of CNN and the temporal data processing capabilities of BiLSTM, enhancing the predictive performance of the model in complex hydrological dynamics. Finally, the study also aims to validate the performance of the Boruta-CNN-BiLSTM model in drought prediction from 2011 to 2020 using actual data from 28 regions in the Huaihe River Basin and compare it with other models to determine its applicability and superiority under different spatial conditions, providing important references and insights for future drought prediction research.

2 Study area and data

2.1 Study area

In this paper, as shown in Fig 1, the Huaihe River Basin is selected as the research area, and the grid is divided at a resolution of 1°lat×1°lon, with a total of 28 grid areas. The Huaihe River Basin is located in eastern China, between 111°55'–121°20' E and 30°55'–36°20' N, covering an area of approximately 270,000 square kilometers. The basin is located in the north-south climate transition zone of China. The north of the Huaihe River is a warm temperate zone, and the south of the Huaihe River is a northern subtropical zone. The climate is mild, and the annual average temperature is 11-16 °C. The temperature change in the basin increases from north to south and from coast to inland. The amount of evaporation is small in the south and large in the north. The annual average water surface evaporation is 900-1500 mm. The average annual precipitation in the Huaihe River Basin is about 920 mm, and its distribution is roughly decreasing from south to north. Mountainous areas are greater than plains, and coastal areas are greater than inland. Due to recurrent droughts in winter and spring, coupled with high temperatures and intense rainfall during summer and autumn, the Huaihe River Basin is highly susceptible to extreme climatic events (Yang et al., 2016). The frequent droughts in the basin cause significant losses to the local area every year. On average, 2.698 million hectares of crops are affected every year, accounting for 21 % of the total area of cultivated land in the basin.

https://doi.org/10.5194/egusphere-2026-1033
Preprint. Discussion started: 2 April 2026

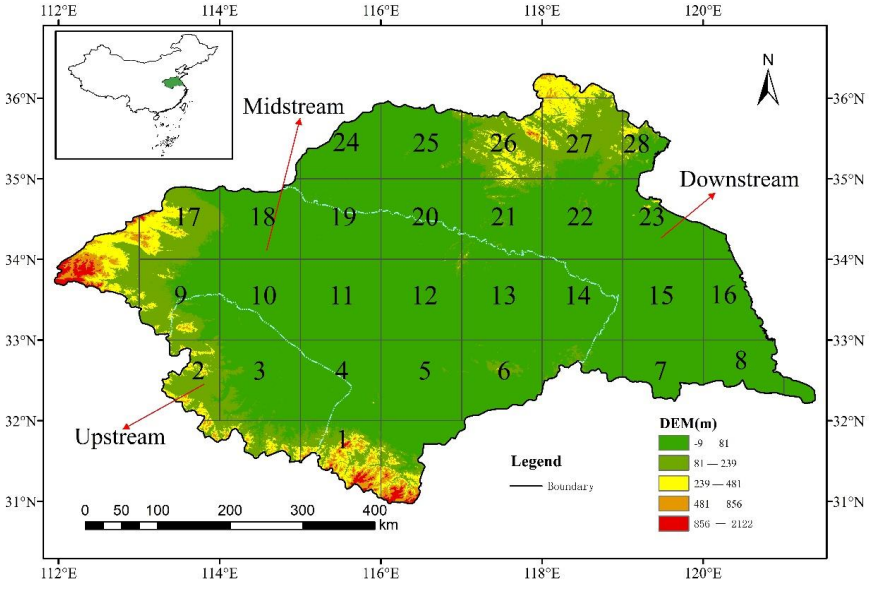

108 **Figure 1: Huaihe River Basin and 28 grid region location.**

109 **2.2 Data**

110 The monthly datasets for rainfall, 2m dewpoint temperature, evapotranspiration, runoff, surface net
111 solar radiation, surface pressure, soil temperature at different depths (0-7cm, 7-28cm, 28-100cm), and
112 Volumetric soil water at different depths (0-7cm, 7-28cm, 28-100cm) for the Huaihe River Basin,
113 covering the period from 1960 to 2020, were obtained from the ERA5-Land reanalysis dataset
114 (https://cds-beta.climate.copernicus.eu/). Grid analysis was conducted at a resolution of 1°lat×1°lon,
115 covering a total of 28 grid points. Using the interpolation method in array, the data of Huaihe River Basin
116 are interpolated into 28 grid regions.

117 In this paper, the potential climate prediction factors for the Huaihe River basin, such as Nino3.4,
118 Atlantic Multidecadal Oscillation (AMO), Pacific Decadal Oscillation (PDO), Arctic Oscillation (AO),
119 and Trans-Niño Index (TNI) data, were obtained from the National Oceanic and Atmospheric
120 Administration (NOAA) website (http://www.esrl.noaa.gov/psd/data/climateindices)(1960-2020).

https://doi.org/10.5194/egusphere-2026-1033
Preprint. Discussion started: 2 April 2026

3 Methods

3.1 Drought index

The standardized runoff index (SRI), as an effective and accurate index to describe hydrological drought characteristics, was first proposed by Shukla and Wood (2008). SRI is a standardized hydrological drought index based on runoff data, which can be used to compare and analyze hydrological drought at different times and spaces. In this study, the SRI-1 index, calculated at a monthly scale, is used as the target variable for predicting hydrological drought conditions. Moreover, SRI is simple in calculation and flexible in use and has been widely used in hydrological drought identification. The calculation method of SRI is as follows:

$$f(x) = \frac{x^{\alpha-1} e^{-\frac{x}{\beta}}}{\beta^{\alpha}\Gamma(\alpha)} \quad (1)$$

$$F(x) = \int_0^x f(x)dx \quad (2)$$

Assuming that the precipitation series x at a certain time scale follows a stationary gamma distribution, where α and β are the scale and shape parameters ($\alpha > 0$, $\beta > 0$). The cumulative probability $F(x)$ of each item is normalized to obtain the corresponding SRI.

3.2 Boruta-feature selection algorithm

Feature selection is a critical step in enhancing the performance of machine learning models, aimed at improving predictive accuracy by selecting the most relevant input features. The Boruta algorithm, an extension of the random forest method, derives its name from the Slavic mythological deity of the forest (Breiman, 2001). Boruta evaluates the importance of each input predictor by comparing it to a set of "shadow features" (randomly generated irrelevant features) using Z-scores, which represent the ratio of mean loss to standard deviation (Kursa et al., 2010). This study utilizes the Boruta algorithm to select significant drought-influencing factors from 31 potential predictors, including climate indices, soil temperature, and precipitation. The algorithm employs a recursive feature elimination strategy, ranking features based on their Z-scores and selecting those with significant contributions. Feature importance is determined by examining the residuals from the Boruta process. In this study, the feature selection

https://doi.org/10.5194/egusphere-2026-1033
Preprint. Discussion started: 2 April 2026

process was implemented using the Boruta package in R, ensuring efficiency and stability in identifying the most significant features for model construction.

3.3 Machine learning models

3.3.1 XGBOOST

The Extreme Gradient Boosting (XGBoost) is an ensemble learning algorithm in the Boosting category. It utilizes decision trees as its fundamental elements and implements the gradient boosting algorithm to minimize loss when adding new models (Chen and Guestrin, 2016). XGBoost is designed to improve both the training speed and the predictive performance of gradient-boosted decision trees. Assuming we have K base models denoted as $f_t(x) \in F$, $t = 1,2,.....,K$, where F is the model space containing all the base models, the XGBoost model can be represented using the following function:

$$\hat{y} = F(x) = \sum_{t=1}^{k} f_t(x) \quad (3)$$

Where the parameters of the XGBoost model consist of the structure of each tree and the scores in the leaf nodes, that is the learning of each function $f_t(x)$.

As each base model is generated in a certain sequential order, the creation of the subsequent tree takes into account the predictions made by the preceding tree. Therefore, the objective function of the t base model can be expressed as follows:

$$y^{(t)} = \sum_{i=1}^{n} l\left(y_i, \hat{y}_i^{(t-1)} + f_t(x_i)\right) + \Omega(f_t) \quad (4)$$

Here, $l\left(y_i, \hat{y}_i^{(t-1)}\right)$ represents the loss function related to $y_i, \hat{y}_i^{(t-1)}$, $y_i^{(t-1)}$ denotes the predictions of the first $t-1$ decision trees for the sample i (i.e., the sum of predictions made by the first $t-1$ trees), y_i represents the actual value of the sample i, $f_t(x_i)$ represents the prediction of the t decision tree for sample i, and $\Omega(f_t)$ represents the model complexity of the t tree. Therefore, the predictions of the first k trees for the sample i are equal to the predictions of the first $k-1$ trees plus the prediction of the k tree.

3.3.2 LSTM

The long short-term memory network (LSTM) model is a variant of recurrent neural network (RNN), which is specifically used to process time series data (Hochreiter and Schmidhuber, 1997). In recording

https://doi.org/10.5194/egusphere-2026-1033
Preprint. Discussion started: 2 April 2026

long-term sequence data, RNN will lead to gradient disappearance or gradient explosion due to the continuous accumulation of information, which makes it difficult for the network to learn long-term dependence (Jaseena and Kovoor, 2021). The LSTM model is designed for this problem. Mainly through the gating mechanism to adjust the information to solve. The LSTM model consists of four interacting layers: input gate, forgetting gate, unit state gate, and output gate, as shown in Figure 2. The input gate determines which new information will be stored in the storage unit. The forgetting door determines which information is forgotten by the memory unit. The cell state is responsible for transmitting and storing long-term memory information so that long-term dependencies can be better captured when processing long-sequence data. The output gate is the neural layer used to calculate the output value at the current moment. The mathematical description of the LSTM model is as follows:

$$i_t = \sigma\left(W_i \cdot \left[h_{t-1}, x_t\right]\right) \tag{5}$$

$$f_t = \sigma(W_f \cdot \left[h_{t-1}, x_t\right] + b_f) \tag{6}$$

$$C_t = f_t \cdot C_{t-1} + i_t \cdot \tanh(W_c \cdot \left[h_{t-1}, x_t\right] + b_f) \tag{7}$$

$$O_t = \sigma(W_o \cdot \left[h_{t-1}, x_t\right] + b_o) \tag{8}$$

Where i, f, C, and O donate the input gate, forget gate, cell state, and output gate, respectively. σ and $\tanh$ donate sigmoid and hyperbolic tangent activation functions, respectively. x_t, t, W, and b donate input vector, time, a weight matrix, and the bias vectors, respectively.

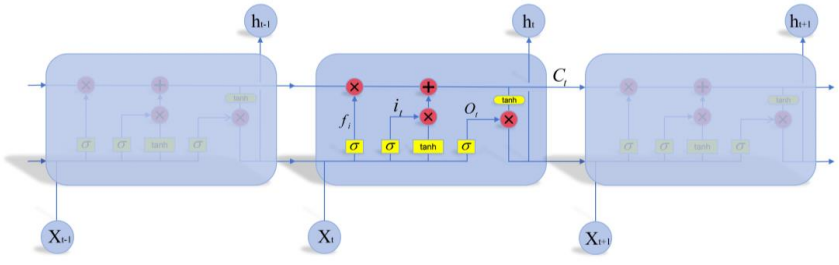

Figure 2: Structure of the LSTM model.

3.3.3 BILSTM

In a traditional unidirectional LSTM model, the input is processed in only one direction, utilizing information derived from past states. In contrast, a Bidirectional Long Short-Term Memory Network (BiLSTM) consists of two layers of LSTM: one processes the input sequence in the forward direction,

https://doi.org/10.5194/egusphere-2026-1033
Preprint. Discussion started: 2 April 2026

while the other analyzes it in the backward direction (Schuster and Paliwal., 1997). The forward layer captures information from previous time steps, whereas the backward layer (also known as the reverse LSTM) captures information from future time steps in the input sequence. Figure 3 shows the BiLSTM model structure.

After passing through both layers, the outputs from the forward and backward passes are combined for further processing. In a BiLSTM network, the hidden state at each time step (h_t) comprises three components: the forward hidden vector (h_t^{forward}), the backward hidden vector (h_t^{backward}), and the current input (x_t). The hidden state for each time step can be represented as follows (Joseph et al., 2022):

$$h_t^{\text{forward}} = \text{LSTM}(x_t, h_{t-1}^{\text{forward}}) \quad (9)$$

$$h_t^{\text{backward}} = \text{LSTM}(x_t, h_{t-1}^{\text{backward}}) \quad (10)$$

$$y_t = \alpha_t h_t^{\text{forward}} + \beta_t h_t^{\text{backward}} + C_t \quad (11)$$

Here, LSTM () refers to the standard mechanism of the LSTM network. The terms α_t and β_t denote the forward and backward output weights of the hidden layer, respectively, while C_t is the bias optimization parameter at time t.

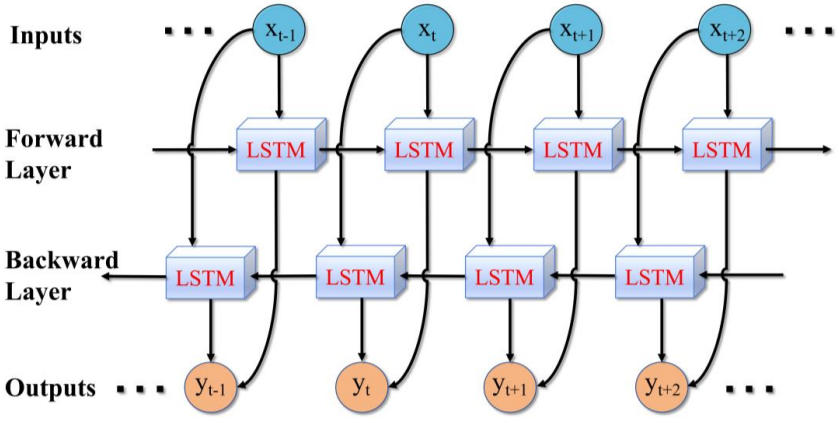

Figure 3: Structure of the BiLSTM model.

3.3.4 CNN-BILSTM

Convolutional Neural Networks (CNNs) are a class of feedforward neural networks characterized by convolutional computation and deep structures. The core idea of CNN is to construct multiple convolutional filters that can extract features from data. Using a hierarchical convolutional structure,

https://doi.org/10.5194/egusphere-2026-1033
Preprint. Discussion started: 2 April 2026

CNNs can capture hidden topological features within input data (Choi and Kil, 2021). As the network depth increases, the extracted features become more abstract. These abstract features are then integrated through fully connected layers and processed by activation functions such as softmax or sigmoid for classification or regression tasks (Li et al., 2024).

CNNs and BiLSTM models are two crucial deep-learning techniques. CNN is more suitable for spatial expansion, which can effectively extract local features and combine them into high-level feature representations. BiLSTM is more suitable for time expansion has strong long-term memory ability and is ideal for processing time scales (Lin et al., 2023). By fully combining the strengths of both approaches, time series data processing can be significantly improved. Figure 4 shows the CNN-BiLSTM hybrid model structure.

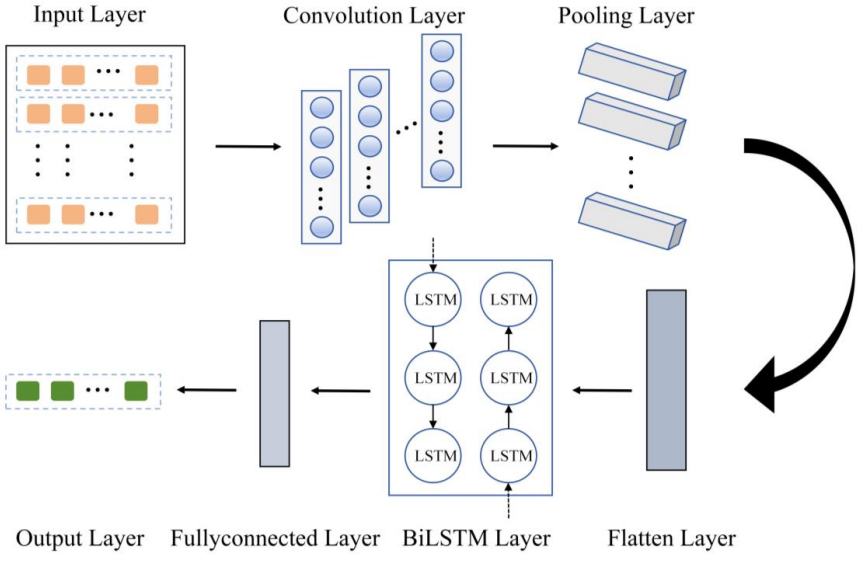

Figure 4: Structure of the CNN-BiLSTM Hybrid Model.

3.4 Hyperparameter tuning

Hyperparameter optimization can improve the performance and efficiency of machine learning model prediction. The Bayesian optimization algorithm using the Bayesian theorem can make full use of the evaluation information of the previous function. It can select the next most promising sampling point according to the posterior distribution of the objective function. The Bayesian optimization algorithm can achieve the global optimal solution of the function with fewer iterations, so it is more suitable for the

https://doi.org/10.5194/egusphere-2026-1033
Preprint. Discussion started: 2 April 2026

hyperparameter search optimization problem of the deep learning model (Wu et al., 2023). The short pseudo-code is shown in Table 1.

Table 1: Algorithm: Bayesian Optimization for Hyperparameter Tuning.

Input: Objective function $f(\,)$, hyperparameter domain X, initial sample size n_0, total budget N
Randomly sample n_0 points $\{x_i\}$ and evaluate $\{y_i = f(x_i)\}$
$D \leftarrow \{(x_i, y_i)\}$
While $\lvert D\rvert < N$:
Train Gaussian Process (GP) on D to obtain mean $\mu_n(x)$ and variance $\sigma_n(x)$
Construct acquisition function $a(x)$
Select next sampling point $x_{\text{next}} = argmax_x a(x)$
Evaluate $y_{\text{next}} = f(x_{\text{next}})$. Train model and compute validation metric.
Update dataset $D \leftarrow D \cup \{(x_{\text{next}}, y_{\text{next}})\}$
end while
Output: optimal hyperparameters corresponding to the best validation metric in D.

3.5 Performance Indicators

This study used five indicators to evaluate the predictive performance of the proposed machine learning model: coefficient of determination (R^2), root mean square error (RMSE), mean absolute error (MAE), mean square error (MSE) and normalized root mean square error (NRMSE). R2 measures the proportion of variance in the observed data interpreted by the model. The closer the value is to 1, the higher the prediction accuracy is. RMSE calculates the square root of the average square difference between the predicted value and the observed value, reflecting the overall size of the prediction error. MAE represents the average absolute difference between the predicted value and the observed value, and describes the accuracy of the model on a more interpretable scale. MSE is the mean of the square difference between the predicted value and the observed value, which emphasizes the larger error. NRMSE is obtained by dividing RMSE by the range of observed values, thus providing a standardized prediction error metric that can be directly compared between different data sets and regions.

These five indicators provide a comprehensive evaluation of model performance from multiple perspectives. These indicators are expressed as follows:

https://doi.org/10.5194/egusphere-2026-1033
Preprint. Discussion started: 2 April 2026

$$R^2 = 1 - \frac{\sum_i (\overline{y_i} - y_i)^2}{\sum_i (\overline{y_i} - y_i)^2} \quad (12)$$

$$RMSE = \sqrt{\frac{1}{n}\sum_{i=1}^{n}(y_i - \hat{y}_i)^2} \quad (13)$$

$$MAE = \frac{1}{n}\sum_{i=1}^{n}|(y_i - \hat{y}_i)| \quad (14)$$

$$MSE = \frac{1}{n}\sum_{i=1}^{n}(y_i - \hat{y}_i)^2 \quad (15)$$

$$NRMSE = \frac{\sqrt{\frac{1}{n}\sum_{i=1}^{n}(y_i - \overline{y_i})^2}}{max(y_i) - min(\overline{y_i})} \quad (16)$$

Where y_i represents the actual observed values, $\overline{y_i}$ is the mean of the actual observed values, $\hat{y}_i$ denotes the predicted values from the model, and n refers to the length of the time series. When the RMSE, MAE, NRMSE, and MSE approach zero, it indicates that the prediction error of the model is minimal. Additionally, when R^2 approaches 1, it suggests that the model demonstrates strong predictive accuracy.

3.6 Convergent Cross Mapping (CCM)

Convergent cross mapping (CCM) is adopted to assess nonlinear causal linkage between a potential driver X and a response Y based on delay-embedding reconstruction (Sugihara et al., 2012). Let $X = \{x(1), x(2), \dots, x(L)\}$ and $Y = \{y(1), y(2), \dots, y(L)\}$ be two monthly time series with $L = 120$. CCM relies on the premise that, if X influences Y, information about Y can be recovered from the manifold reconstructed from X, and such recovery skill should increase and stabilize as the library size grows. Given the assumed one-way influence, X is treated as the cause and the predicted SRI-1 series is treated as the effect Y. The simple procedural steps for the calculation of CCM are presented as follows:

(1) Reconstruct the shadow manifold. A delay-embedded vector is formed from X to represent the system state:

$$x(t) = \{X(t), X(t-\tau), \dots, X(t-(E-1)\tau)\}, t = 1 + (E-1)\tau, \dots, L \quad (17)$$

where E is the embedding dimension and τ is the lag step. The $\tau = 2$ and the $E = 3$ is adopted in this study.

(2) Search nearest neighbors and assign weights. For each point $x(t)$ on M_x, its $E+1$ nearest neighbors $x(t_i)$ are identified based on Euclidean distances $d[x(t), x(t_i)]$. The weights are computed as:

$$w_i = \frac{m_i}{\sum_{j=1}^{E+1} m_j}, (i = 1,2, \dots, E+1) \quad (18)$$

https://doi.org/10.5194/egusphere-2026-1033
Preprint. Discussion started: 2 April 2026

$$m_i = exp^{-\frac{d[x(t),x(t_i)]}{d[x(t),x(t_1)]}} \quad (19)$$

where t_1 is the index of the closest neighbor.

(3) Estimate Y via cross mapping. Using the weighted neighbors, the cross-mapped estimate of Y is obtained by:

$$\hat{y}(t)|M_x = \sum_{i=1}^{E+1} w_i y(t_i) \quad (20)$$

(4) Evaluate cross-map skill and test convergence. The CCM skill is measured by the correlation ρ between $\hat{y}(t)|M_x$ and the original Y. Causality is supported only when ρ shows a convergent pattern with increasing library size. In this study, the coefficient of variation $C_v < 0.1$ is used as a necessary criterion to indicate convergence (Zhou et al., 2023). Given the assumed one-way influence, the drivers are treated as the cause (X) and the predicted SRI-1 series is treated as the effect (Y); the converged ρ is interpreted as the causal strength.

4 Results

To validate the performance of the proposed machine learning hybrid model, the proposed model predicts hydrological drought conditions in 28 grid regions of the Huaihe River Basin using monthly scale data of different drought-influencing factors from 1960 to 2020. The calibration period of the model is from 1960 to 2010, and the verification period is from 2011 to 2020. To construct six different machine learning models for each grid region, the Boruta feature selection algorithm was applied to select relevant drought-influencing factors from a total of 31 drought-influencing factors. The selected features were then inputted into six machine learning models, with the output value being a 1-month time scale SRI(SRI-1). Due to space constraints, this study takes four representative grid regions as the analysis object, which are the 1st, 7th, 17th, and 21st regions.

Table 2: Drought influencing factors input by the Boruta feature selection algorithm (T is the lead time, SPI-1, SPI-3, SPI-6, and SPI-9 are SPI values at different monthly scales).

Drought influencing factors	
1	SPI-1
2	SPI-3
3	SPI-6
4	SPI-9
5	T=1 SPI-1
6	T=1 SPI-3
7	T=1 SPI-6

https://doi.org/10.5194/egusphere-2026-1033
Preprint. Discussion started: 2 April 2026

8	T=1 SPI-9
9	T=2 SPI-1
10	T=2 SPI-3
11	T=2 SPI-6
12	T=2 SPI-9
13	T=3 SPI-1
14	T=3 SPI-3
15	T=3 SPI-6
16	T=3 SPI-9
17	d2m temperature
18	surface pressure
19	evapotranspiration
20	surface net solar radiation (SNSR)
21	soil temperature (0-7cm) (STL1)
22	soil temperature (7-28cm) (STL2)
23	soil temperature (28-100cm) (STL3)
24	volumetric soil water (0-7cm) (VSW1)
25	volumetric soil water (7-28cm) (VSW2)
26	volumetric soil water (28-100cm) (VSW3)
27	Nino3.4
28	AMO
29	PDO
30	AO
31	TNI

4.1 Feature selection

To enhance the prediction performance of the model, 35 drought-influencing factors are selected using the Boruta feature selection algorithm. Figure 5 and Figure 6 show Boruta feature selection results in four grid regions. Green represents the features that have a significant contribution to the model prediction results, and these features are considered important. Red represents unimportant features, indicating that these features have no significant contribution to model prediction. Blue represents shadow features, which are randomly disrupted features for comparison with actual features to determine whether actual features are more important than random features. Yellow represents the undetermined feature, that is, the importance of the feature is uncertain. In this paper, the Boruta feature algorithm selects the significant contribution features of green representatives. Boruta feature selection plays a key role in improving model accuracy by reducing feature redundancy. The selected features, such as SPI-1, evapotranspiration, and soil temperature, have important contributions to the predictive ability of the model. Among them, SPI-1 was found to be the most influential feature in all regions, and its importance

https://doi.org/10.5194/egusphere-2026-1033
Preprint. Discussion started: 2 April 2026

score exceeded 30, which was much higher than other features, highlighting its importance in hydrological drought prediction. This shows that the addition of relevant climate indices significantly improves the prediction ability of the model in different spatial backgrounds.

https://doi.org/10.5194/egusphere-2026-1033
Preprint. Discussion started: 2 April 2026

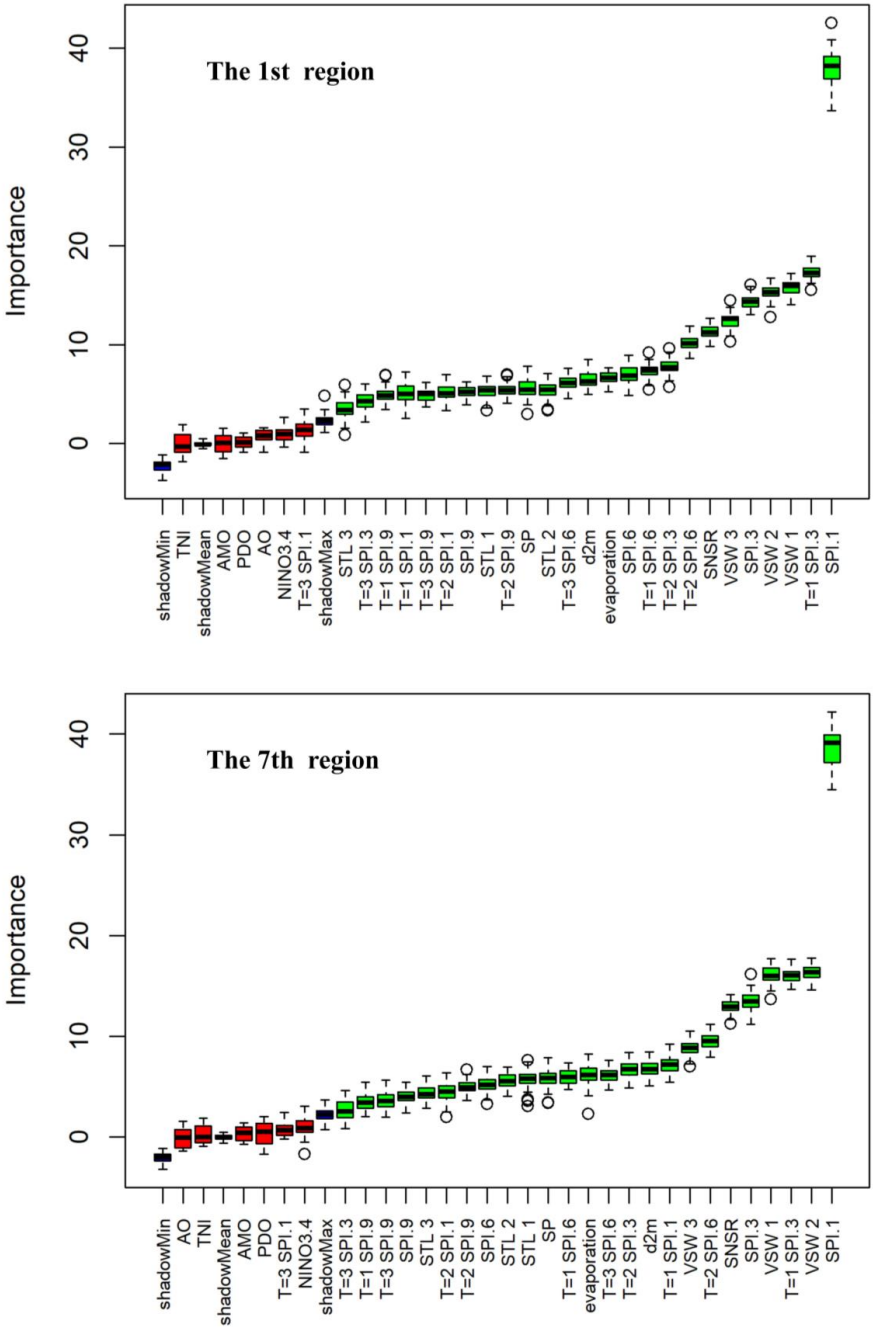

313 **Figure 5: The Boruta feature selection results of the 1st and 7th grid regions (SPI.n are SPI values at**
314 **different monthly scales, n=1,3,6,9).**

https://doi.org/10.5194/egusphere-2026-1033
Preprint. Discussion started: 2 April 2026

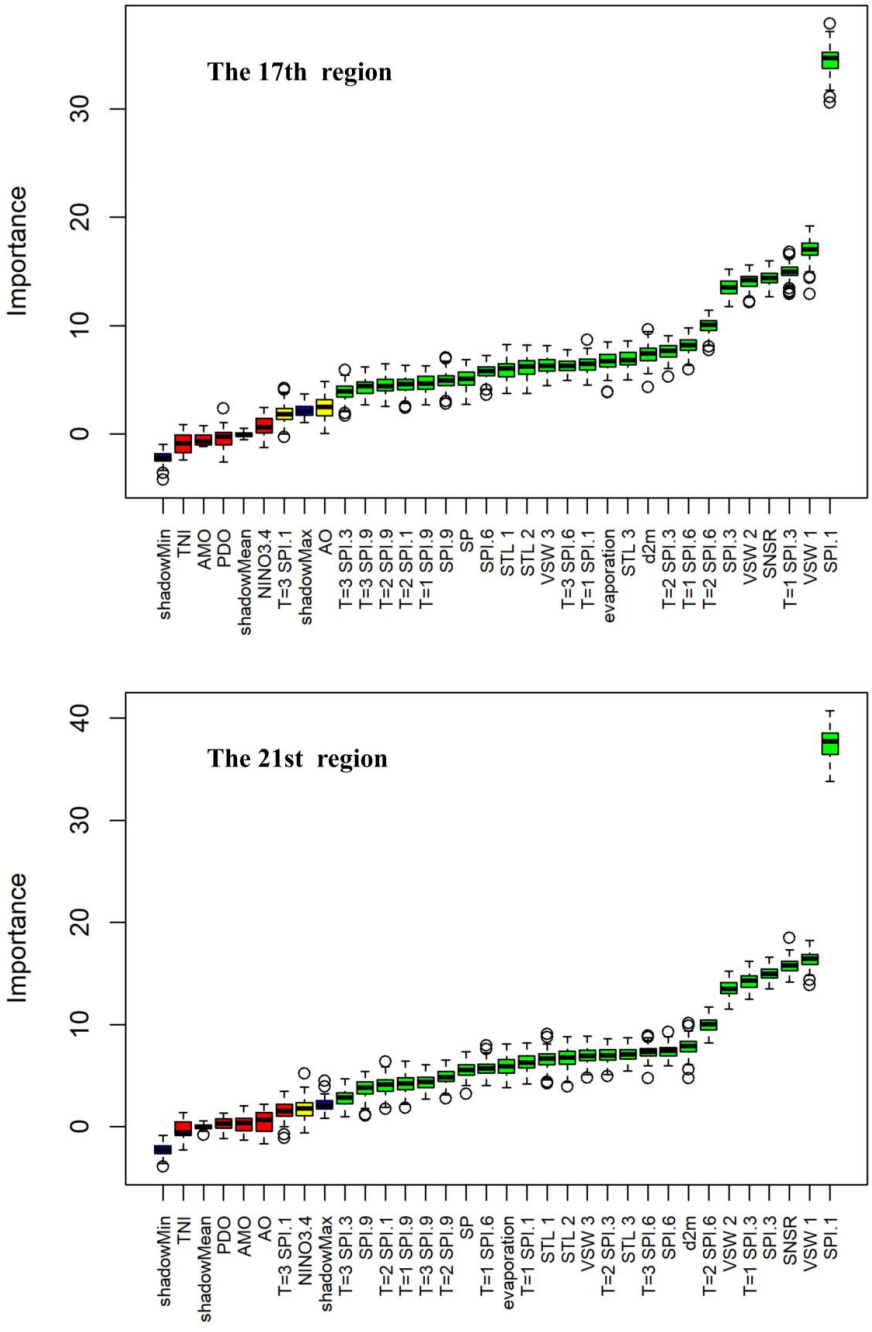

315 **Figure 6: The Boruta feature selection results in the 17th and 21st grid regions (SPI.n are SPI values at**
316 **different monthly scales, n=1,3,6,9).**

317

https://doi.org/10.5194/egusphere-2026-1033
Preprint. Discussion started: 2 April 2026

4.2 Model parameters optimization

In this study, Bayesian optimization is used to fine-tune the hyperparameters of each model to ensure optimal performance. Table 3 shows the optimized parameters of the six models in the 7th grid region. For example, in the Boruta-CNN-BiLSTM model, a learning rate of 0.0023 is selected, and 38 Bi LSTM hidden units and 31 convolutional filters are configured to achieve an optimal balance between model complexity and generalization ability. This highlights the importance of model parameterization in effectively capturing cross-regional hydrological dynamics.

Table 3: Parameters of six models in the 7th grid region after Bayesian optimization.

Model	Parameters
Boruta-CNN-BiLSTM	learningRate:0.0023; BiLSTM numUnits:38; convFilterSize:22; convNumFilters:31; poolSize:2; MaxEpochs:116; dropoutRate:0.34
Boruta-CNN-LSTM	learningRate:0.0038; LSTM numUnits:27; convFilterSize:25; convNumFilters:7; poolSize:4; MaxEpochs:182; dropoutRate:0.22
Boruta-CNN-XGBoost	convFilterSize:3; convNumFilters:13; poolSize:2; num_Trees: 244; eta: 0.177; max_depth:6
Boruta-BiLSTM	numUnits:3; learningRate:0.0216; dropoutRate:0.26; MaxEpochs:216
Boruta-LSTM	numUnits1:10; numUnits2:50; numUnits3:50; learningRate:0.0732; dropoutRate:0.16; MaxEpochs:188
Boruta-XGBoost	eta:0.0746; max_depth:2; num_trees:895

4.3 Model evaluation

Figure 7 shows the average improvement of the prediction performance of each model after using the Boruta algorithm to filter features. It can be seen from the figure that the prediction performance of all models has improved, among which the Boruta-CNN-BiLSTM model has the most significant improvement: RMSE decreased by 12.633%, MAE decreased by 14.689%, and R2 increased by 4.650%. For other models, for example, the RMSE and MAE of the Boruta-CNN-XGBoost model are reduced by 12.215% and 12.830%, respectively, while the Boruta-XGBoost model has the smallest performance improvement, and the RMSE is only reduced by 2.434%. This shows that the combination of the Boruta feature selection method can effectively reduce the feature redundancy of the model and improve the stability and prediction accuracy of the model under complex hydrological conditions.

https://doi.org/10.5194/egusphere-2026-1033
Preprint. Discussion started: 2 April 2026

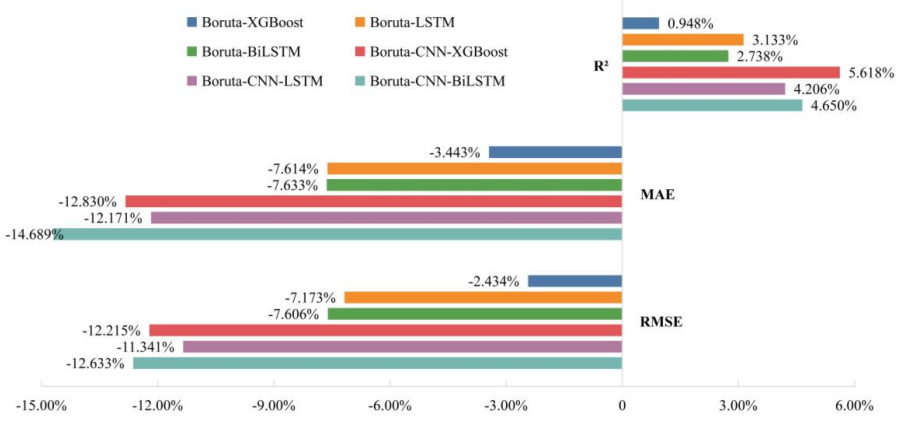

Figure 7: The improvement of prediction performance of various models after the application of the Boruta algorithm (The data presented represent the average performance improvement of each model in 28 grid regions).

Table 4 shows the average values of five evaluation indexes (RMSE, NRMSE, MSE, MAE, R^2) of the six models in 28 grid regions. The Boruta-CNN-BiLSTM achieved the lowest average error and the highest R^2, confirming its leading performance. Boruta-CNN-LSTM is sub-optimal, while Boruta-BiLSTM ranks third. Tree-based models and single LSTM perform worse and have higher errors. As shown in Figure 8, Boruta-CNN-BiLSTM dominates in almost all regions, although Boruta-CNN-LSTM obtains slightly higher R^2 in one region, while Boruta-BiLSTM is slightly better in some other regions, which is consistent with Table 4.

In addition, the Boruta-CNN-BiLSTM and Boruta-CNN-LSTM models are superior to the models without CNN, while the Boruta-CNN-XGBoost model shows the highest error, reflecting its limitations in capturing complex nonlinear dynamics. These comparisons confirm that combining CNN with appropriate deep learning and feature selection produces the most robust model.

https://doi.org/10.5194/egusphere-2026-1033
Preprint. Discussion started: 2 April 2026

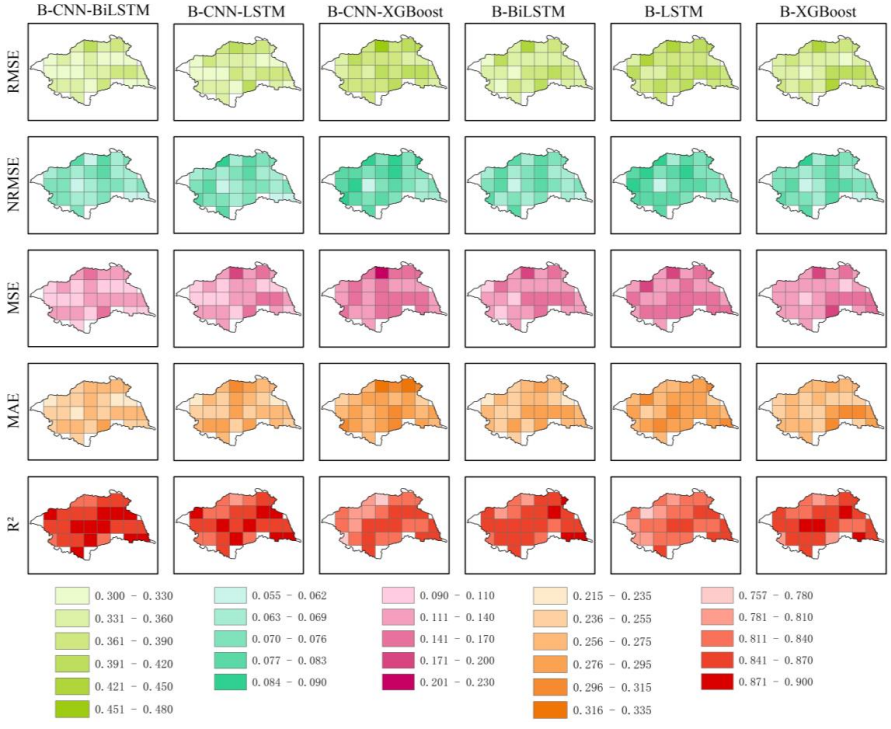

Figure 8: The spatial distribution of five evaluation metrics for the six models across the 28 grid regions.

Table 4: The average value of five evaluation indexes of six models in 28 grid regions.

Model	RMSE	NRMSE	MSE	MAE	R^2
Boruta-CNN-BiLSTM	**0.341**	**0.069**	**0.117**	**0.252**	**86.31%**
Boruta-CNN-LSTM	0.352	0.071	0.125	0.262	85.35%
Boruta-CNN-XGBoost	0.38	0.077	0.145	0.284	82.93%
Boruta-BiLSTM	0.357	0.072	0.128	0.263	84.89%
Boruta-LSTM	0.383	0.077	0.147	0.279	82.66%
Boruta-XGBoost	0.364	0.073	0.134	0.277	84.38%

https://doi.org/10.5194/egusphere-2026-1033
Preprint. Discussion started: 2 April 2026

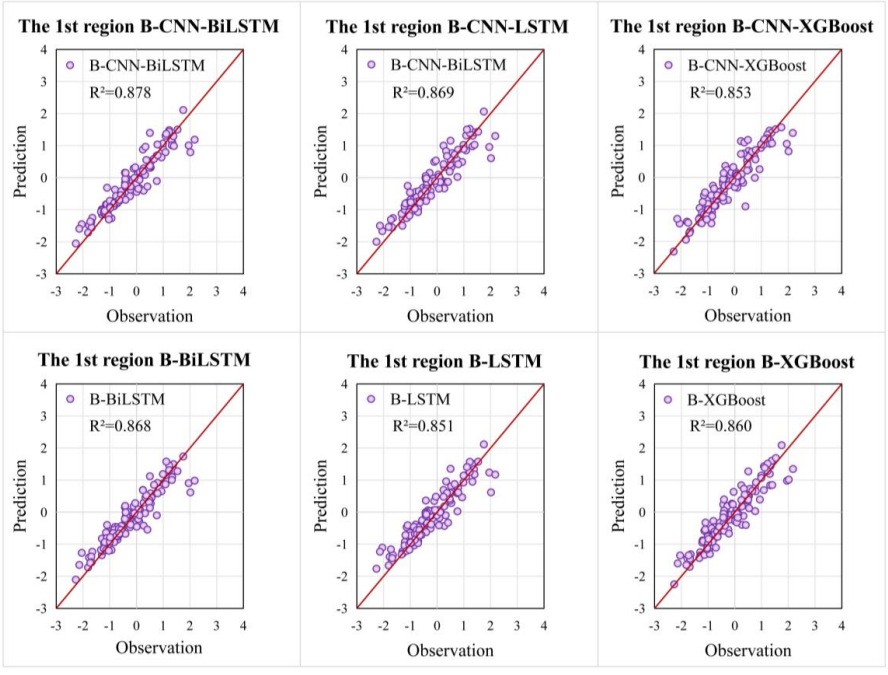

353 **Figure 9: Scatter plot of the 1st grid region model prediction.**

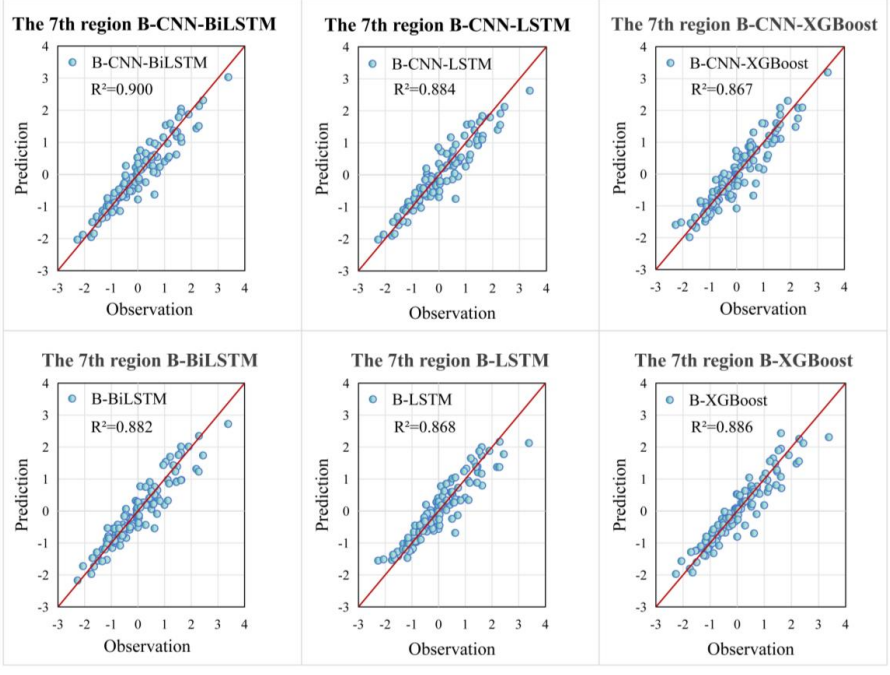

354 **Figure 10: Scatter plot of the 7th grid region model prediction.**

https://doi.org/10.5194/egusphere-2026-1033
Preprint. Discussion started: 2 April 2026

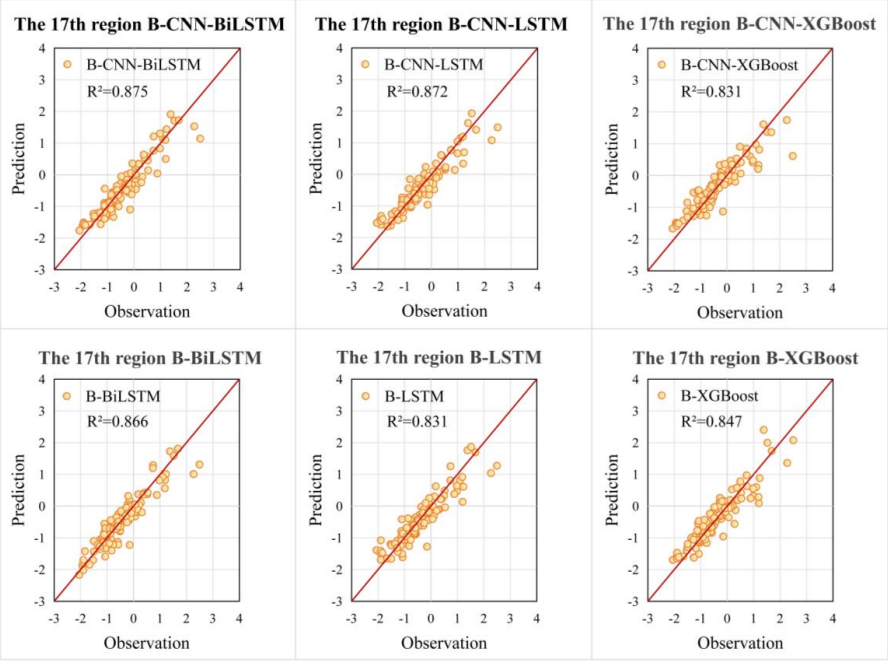

355 **Figure 11: Scatter plot of the 17th grid region model prediction.**

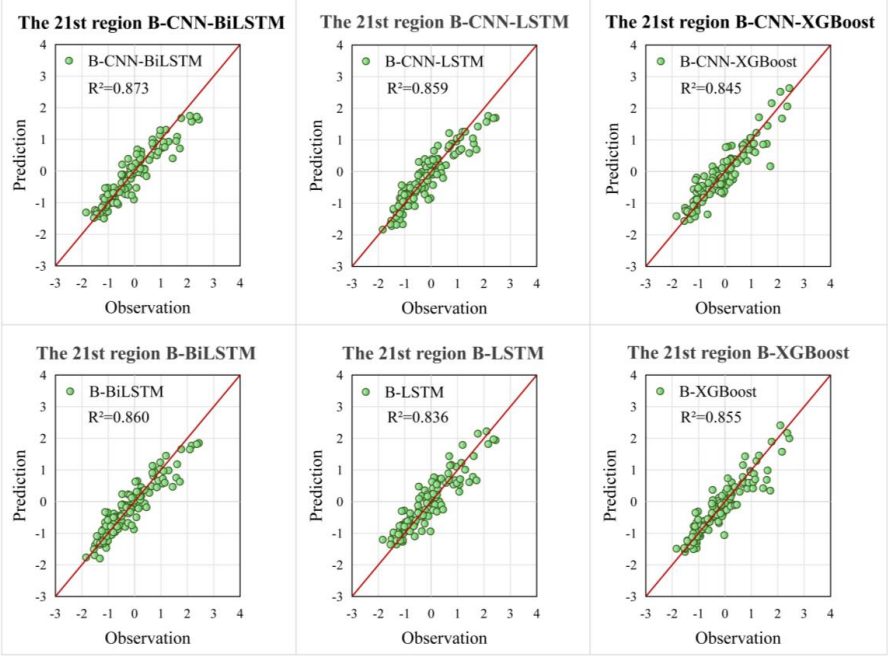

356 **Figure 12: Scatter plot of the 21st grid region model prediction.**

https://doi.org/10.5194/egusphere-2026-1033
Preprint. Discussion started: 2 April 2026

To further assess and compare the accuracy of hydrological drought predictions for each model, the predicted and measured values of each model were linearly fitted. Taking four regions as examples, the scatter plots of the predicted and measured values of the model in each region are shown in Figures 9-12. It can be seen that in the four regions, the predicted values of the Boruta-CNN-BiLSTM model are closely gathered around the diagonal, indicating that the predicted values are in good agreement with the actual values. In addition, the predictions of the Boruta-CNN-LSTM model in the 1st, 7th, and 17th grid regions and the Boruta-BiLSTM model in the 21st region are also close to the diagonal. In contrast, the Boruta-LSTM model in the 1st, 17th, and 21st grid regions and the Boruta-CNN-XGBoost model in the 7th grid region show more data points scattered around the diagonal, indicating weaker performance than the Boruta-CNN-BiLSTM.

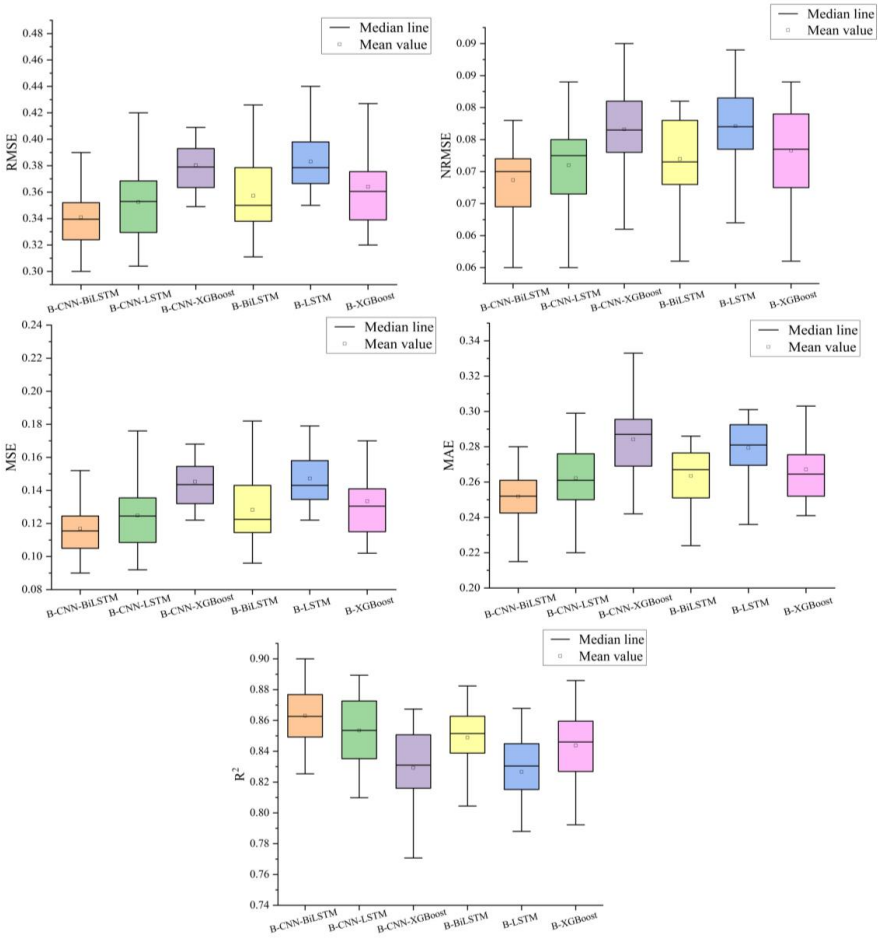

Figure 13: Box plots of six models about five indicators.

https://doi.org/10.5194/egusphere-2026-1033
Preprint. Discussion started: 2 April 2026

In order to provide a comprehensive comparison of model performance, Figure 13 shows a box plot of five evaluation indicators (RMSE, MAE, MSE, NRMSE, R^2) of six models in all regions. It can be seen that the Boruta-CNN-BiLSTM model has always achieved the lowest error value and the highest R^2 value, highlighting its superiority over other models. Specifically, most of the RMSE values remain below 0.35, and the MAE values are generally below 0.26, while MSE and NRMSE remain at the lowest levels in the whole model. This shows that the Boruta-CNN-BiLSTM model not only minimize absolute deviation and square deviation, but also maintains a stable normalized error, thus ensuring robustness and comparability between different regions. In contrast, the Boruta-CNN-XGBoost model showed the highest error level among all indicators, reflecting weak predictive performance. For BiLSTM and LSTM models, prediction accuracy is significantly improved after adding CNN, which confirms the role of CNN in improving spatial feature extraction and model robustness.

Figure 14 further illustrates the predictive accuracy of the six models using Taylor diagrams in four representative grid regions (1st, 7th, 17th, and 21st). The Boruta-CNN-BiLSTM model produces predictions most closely aligned with the observed data, showing the highest correlation coefficients and the smallest deviations in all four regions. In the 1st, 17th and 21st grids, the Boruta-BiLSTM model ranks second in accuracy, while in the 7th grid, the Boruta-CNN-LSTM model is the second best model. These results once again highlight the comprehensive advantages of the Boruta-CNN-Bi LSTM model, which combines effective feature selection with strong spatio-temporal expression ability, thus achieving superior performance across multiple evaluation indicators and regional conditions.

https://doi.org/10.5194/egusphere-2026-1033
Preprint. Discussion started: 2 April 2026

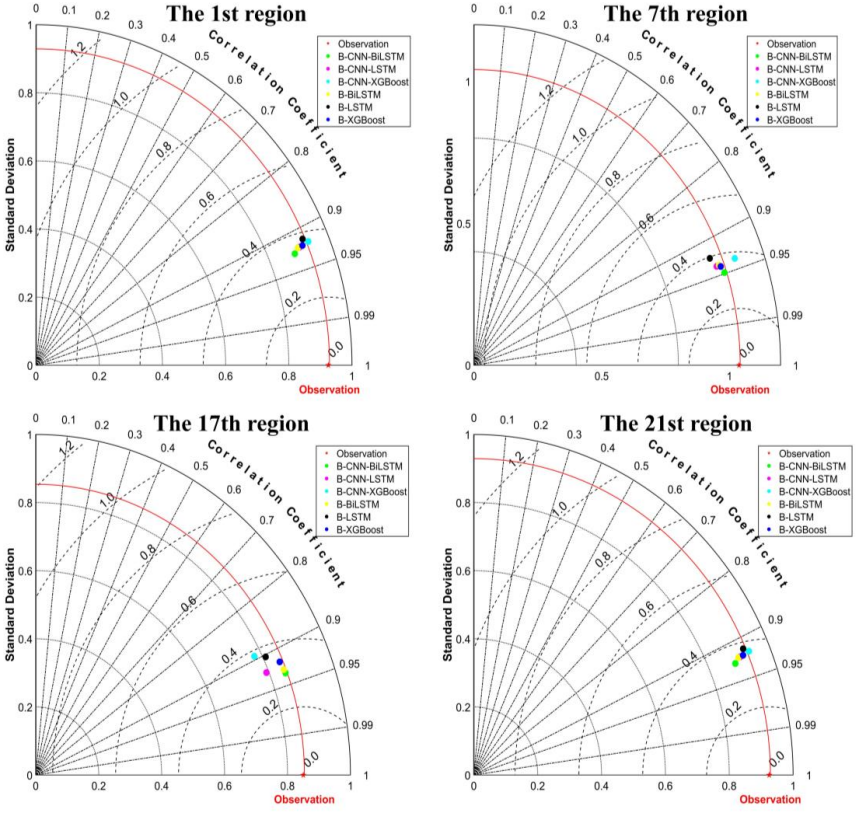

Figure 14: The Taylor diagrams of the six models in the 1st, 7th, 17th, and 21st grid regions.

5 Discussion

In order to analyze the reasons for the spatial differences in the prediction accuracy of the Boruta-CNN-BiLSTM model, the most influential factors obtained by the Boruta method were selected, namely precipitation, volumetric soil water (0-7cm), volumetric soil water (7-28cm) and surface net solar radiation. The CCM method was used to quantify the impacts of each influencing factor on the model evaluation index R^2. The results are shown in Figures 16 and 17. According to Figures 15, 16 and 17, precipitation is the most significant influencing factor affecting the prediction accuracy of the model across the entire watershed. The mean value of the ρ-value is close to 0.9, and the range is mainly between 0.8 and 1.0. The data are relatively concentrated, which indicates that the model's prediction accuracy is sensitive to precipitation and is distributed relatively uniformly in space. However, the precipitation is unevenly distributed across the basin, with more in the south and less in the north. VSW1 and VSW2 are

https://doi.org/10.5194/egusphere-2026-1033
Preprint. Discussion started: 2 April 2026

401 factors that have a greater impact on model prediction accuracy after precipitation. The mean ρ-value
402 ranging from 0.4 to 0.5, and the range is mainly between 0.2 and 0.7. The wide range of data distribution
403 indicates that the sensitivity of the model's prediction accuracy to precipitation varies significantly in
404 space. The specific manifestation is that the sensitivity in the upper and middle reaches is greater than
405 that in the downstream areas. The distribution of VSW1 and VSW2 across the basin is also uneven, its
406 distribution is consistent with the partial sensitivity. The factor that has the least impact on the model's
407 prediction accuracy is SNSR, with a mean close to 0.2 and a distribution range between 0 and 0.4. This
408 study analyzed the SRI based on a 1-month time scale, constructed several different prediction models,
409 and conducted evaluations. This study analyzed the SRI based on a one-month time scale, constructed
410 several prediction models, and evaluated the effectiveness of the prediction models from multiple aspects.
411 The results show that the Boruta-CNN-BiLSTM model has the most effective prediction effect. However,
412 the SRI on different time scales may have a significant impact on the performance of the prediction model.
413 In addition to that, drought is also affected by human activities, basin geographical features, etc. For
414 future research, the uncertainty of the model's prediction performance due to different time scales and
415 various influence factors can be considered.

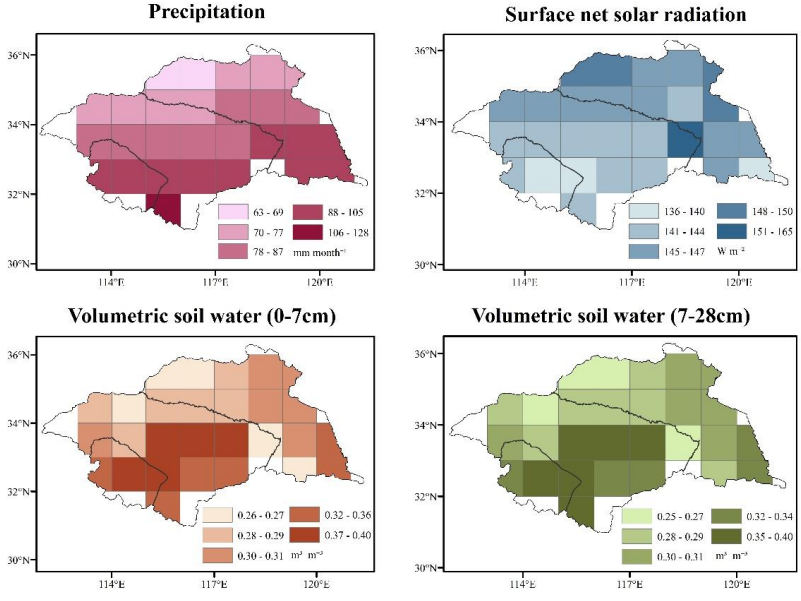

416
417 **Figure 15: Spatial distribution maps of monthly mean values of precipitation, volumetric soil water (0-7cm),**
418 **volumetric soil water (7-28cm) and surface net solar radiation in the basin from 1960 to 2010.**

https://doi.org/10.5194/egusphere-2026-1033
Preprint. Discussion started: 2 April 2026

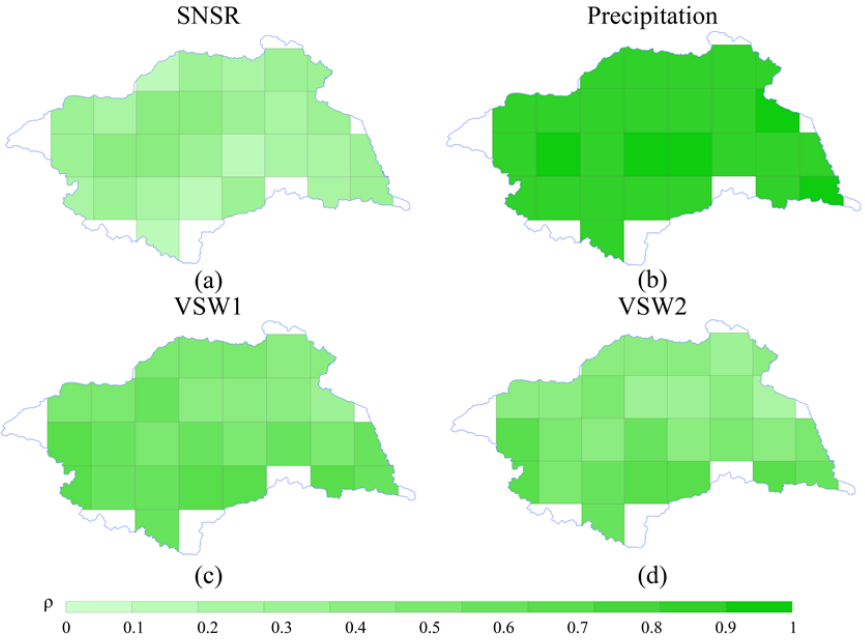

Figure 16: Spatial distribution of the influence intensity (ρ) of precipitation, volumetric soil water (0-7cm) (VSW1), volumetric soil water (7-28cm) (VSW2) and surface net solar radiation (SNSR) on the prediction accuracy of the Boruta-CNN-BiLSTM model.

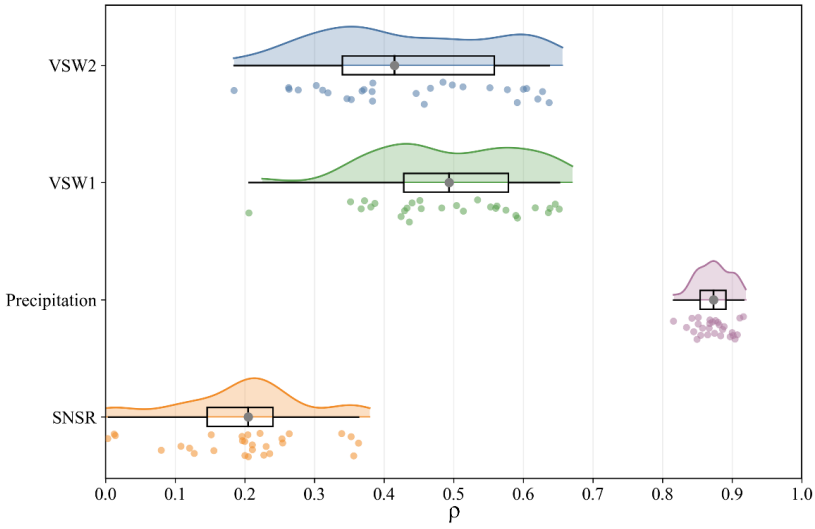

Figure 17: Raincloud plots of the influence intensity (ρ) of different factors on the prediction accuracy of the Boruta-CNN-BiLSTM model.

https://doi.org/10.5194/egusphere-2026-1033
Preprint. Discussion started: 2 April 2026

6 Conclusion

This paper proposes an innovative hydrological drought prediction model called Boruta-CNN-BiLSTM, which is a hybrid model of the Boruta feature selection algorithm, a bidirectional long- and short-term memory network (BiLSTM), and a convolutional neural network (CNN). It is used to predict hydrological drought in the Huaihe River Basin in China. In addition, five models, Boruta-CNN-LSTM, Boruta-CNN-XGBoost, Boruta-BiLSTM, Boruta-LSTM, and Boruta-XGBoost were established for comparison. The main conclusions are as follows:

(1) The addition of Boruta significantly improved all benchmark models. Among the six models, Boruta-CNN-BiLSTM showed the largest gain, with an average RMSE decrease of 0.42, a mean MAE decrease of 0.32, an average NRMSE decrease of 0.008, a mean MSE decrease of 0.03, and a median R^2 increase of 3.65%. It highlights the importance of optimizing feature selection for robust prediction.

(2) Boruta-CNN-BiLSTM achieved the highest overall accuracy across all regions. The next best is Boruta-CNN-LSTM. Boruta-LSTM model performs the poorest. Boruta-BiLSTM, Boruta-CNN-XGboost and Boruta-XGboost perform in the middle. These results highlight the robustness of this hybrid approach to capturing the spatial and temporal dynamics associated with hydrological droughts. Compared with other models, the model effectively characterizes complex hydrological patterns and significantly improves drought prediction accuracy in the Huaihe River Basin.

(3) The prediction effect of the Boruta-CNN-BiLSTM model is mainly influenced by factors such as precipitation, volumetric soil water (0-7cm), volumetric soil water (7-28cm) and surface net solar radiation. Among them, precipitation has an absolute dominant influence throughout the entire watershed, and the influence varies a little in the spatial distribution of the watershed. Volumetric soil water (0-7cm) and volumetric soil water (7-28cm) follow, and their influences on the model's prediction effect have certain spatial differences. The influence in the middle and upper reaches is more significant than in downstream areas. SNSR has the least influence on the model's prediction effect among the four influencing factors.

Statements & Declarations

Funding

This work was supported by Open Research Fund Program of National Key Laboratory of Water

https://doi.org/10.5194/egusphere-2026-1033
Preprint. Discussion started: 2 April 2026

Disaster Prevention (grant no. 2024490711), Yangzhou University Graduate Student Research and Practice Innovation Program Funding projects (grant no. SJCX24_2250), and Natural Science Foundation of Jiangsu Province (grant no. BK20250906).

Competing Interests

The authors declare no conflict of interest.

Author Contributions

All authors contributed this paper: Conceptualization, M L, YH Y; Data curation, YH Y, M L, M O, CM Y; Visualization, YH Y, M L; Validation, M L, YH Y; Methodology, M L, YH Y, M O; Formal Analysis, M L, YH Y; Funding acquisition, M L, YH Y; Writing – original draft, YH Y; Writing – review & editing, M L.

Data availability

We are grateful to the National Oceanic and Atmospheric Administration (http://www.esrl.noaa.gov/psd/data/climateindices) for providing large-scale climate index data, and the European Centre for Medium-Range Weather Forecasts (https://cds.climate.copernicus.eu/) for providing monthly mean precipitation, volumetric soil water, evapotranspiration, 2m dewpoint temperature, surface net solar radiation, surface pressure and runoff datasets. The data and materials of this study are available.

Reference

Achite, M., Emami, S., Jehanzaib, M., Katipoglu, O. M., and Emami, H.: An election algorithm combined with support vector regression for estimating hydrological drought, MODELING EARTH SYSTEMS AND ENVIRONMENT, https://doi.org/10.1007/s40808-023-01850-y, 2023.

Ahmed, A. A. M., Deo, R. C., Feng, Q., Ghahramani, A., Raj, N., Yin, Z., and Yang, L.: Deep learning hybrid model with Boruta-Random forest optimiser algorithm for streamflow forecasting with climate mode indices, rainfall, and periodicity, JOURNAL OF HYDROLOGY, 599, 126350, https://doi.org/10.1016/j.jhydrol.2021.126350, 2021.

Apurv, T., Sivapalan, M., and Cai, X.: Understanding the Role of Climate Characteristics in Drought Propagation, WATER RESOURCES RESEARCH, 53, 9304–9329, https://doi.org/10.1002/2017WR021445, 2017.

Ardabili, S., Mosavi, A., Dehghani, M., and Várkonyi-Kóczy, A. R.: Deep Learning and Machine Learning in Hydrological Processes Climate Change and Earth Systems a Systematic Review, in: Engineering for Sustainable Future, 52–62, 2020.

https://doi.org/10.5194/egusphere-2026-1033
Preprint. Discussion started: 2 April 2026

485 Breiman, L.: Random Forests, Machine Learning, 45, 5–32, https://doi.org/10.1023/A:1010933404324,
486 2001.

487 Chen, T. and Guestrin, C.: XGBoost: A Scalable Tree Boosting System, in: Proceedings of the 22nd ACM
488 SIGKDD International Conference on Knowledge Discovery and Data Mining, San Francisco, California,
489 USA, 785–794, https://doi.org/10.1145/2939672.2939785, 2016.

490 Chen, Z., Wang, G., Wei, X., Liu, Y., Duan, Z., Hu, Y., and Jiang, H.: Basin-Scale Daily Drought
491 Prediction Using Convolutional Neural Networks in Fenhe River Basin, China, ATMOSPHERE, 15, 155,
492 https://doi.org/10.3390/atmos15020155, 2024.

493 Choi, Y. R. and Kil, R. M.: Face Video Retrieval Based on the Deep CNN With RBF Loss, IEEE
494 TRANSACTIONS ON IMAGE PROCESSING, 30, 1015–1029,
495 https://doi.org/10.1109/TIP.2020.3040847, 2021.

496 Christ, M., Kempa-Liehr, A. W., and Feindt, M.: Distributed and parallel time series feature extraction
497 for industrial big data applications, 2017.

498 Dikshit, A. and Pradhan, B.: Interpretable and explainable AI (XAI) model for spatial drought prediction,
499 SCIENCE OF THE TOTAL ENVIRONMENT, 801, 149797,
500 https://doi.org/10.1016/j.scitotenv.2021.149797, 2021.

501 Elbeltagi, A., Pande, C. B. B., Kumar, M., Tolche, A. D., Singh, S. K., Kumar, A., and Vishwakarma, D.
502 K.: Prediction of meteorological drought and standardized precipitation index based on the random forest
503 (RF), random tree (RT), and Gaussian process regression (GPR) models, ENVIRONMENTAL
504 SCIENCE AND POLLUTION RESEARCH, 30, 43183–43202, https://doi.org/10.1007/s11356-023-
505 25221-3, 2023.

506 Gyaneshwar, A., Mishra, A., Chadha, U., Vincent, P. M. D. R., Rajinikanth, V., Ganapathy, G. P., and
507 Srinivasan, K.: A Contemporary Review on Deep Learning Models for Drought Prediction,
508 SUSTAINABILITY, 15, 6160, https://doi.org/10.3390/su15076160, 2023.

509 Hochreiter, S. and Schmidhuber, J.: Long Short-Term Memory, Neural Computation, 9, 1735–1780,
510 https://doi.org/10.1162/neco.1997.9.8.1735, 1997.

511 Jaseena, K. U. and Kovoor, B. C.: Decomposition-based hybrid wind speed forecasting model using deep
512 bidirectional LSTM networks, ENERGY CONVERSION AND MANAGEMENT, 234, 113944,
513 https://doi.org/10.1016/j.enconman.2021.113944, 2021.

514 Joseph, R. V., Mohanty, A., Tyagi, S., Mishra, S., Satapathy, S. K., and Mohanty, S. N.: A hybrid deep
515 learning framework with CNN and Bi-directional LSTM for store item demand forecasting, Computers
516 and Electrical Engineering, 103, 108358, https://doi.org/10.1016/j.compeleceng.2022.108358, 2022.

517 Kadapala, B. K. R., Farsana, M. A., Vimala, C. H. G., Joshi, S., Hakeem, K. A., and Raju, P. V.: A grid-
518 wise approach for accurate computation of Standardized Runoff Index (SRI), SCIENCE OF THE TOTAL
519 ENVIRONMENT, 946, 174472, https://doi.org/10.1016/j.scitotenv.2024.174472, 2024.

https://doi.org/10.5194/egusphere-2026-1033
Preprint. Discussion started: 2 April 2026

Karbasi, M., Ali, M., Bateni, S. M., Jun, C., Jamei, M., and Yaseen, Z. M.: Boruta extra tree-bidirectional long short-term memory model development for Pan evaporation forecasting: Investigation of arid climate condition, ALEXANDRIA ENGINEERING JOURNAL, 86, 425–442, https://doi.org/10.1016/j.aej.2023.11.061, 2024.

Khan, N., Sachindra, D. A., Shahid, S., Ahmed, K., Shiru, M. S., and Nawaz, N.: Prediction of droughts over Pakistan using machine learning algorithms, ADVANCES IN WATER RESOURCES, 139, 103562, https://doi.org/10.1016/j.advwatres.2020.103562, 2020.

Kheyruri, Y., Sharafati, A., and Neshat, A.: Predicting agricultural drought using meteorological and ENSO parameters in different regions of Iran based on the LSTM model, STOCHASTIC ENVIRONMENTAL RESEARCH AND RISK ASSESSMENT, 37, 3599–3613, https://doi.org/10.1007/s00477-023-02465-6, 2023.

KUBIAK-WOJCICKA, K. and JUSKIEWICZ, W.: Relationships between meteorological and hydrological drought in a young-glacial zone (north-western Poland) based on Standardised Precipitation Index (SPI) and Standardized Runoff Index (SRI), ACTA MONTANISTICA SLOVACA, 25, 517–531, https://doi.org/10.46544/AMS.v25i4.07, 2020.

Kursa, M. B., Jankowski, A., and Rudnicki, W. R.: Boruta - A System for Feature Selection, 2010.

Kuswanto, H. and Naufal, A.: Evaluation of performance of drought prediction in Indonesia based on TRMM and MERRA-2 using machine learning methods, METHODSX, 6, 1238–1251, https://doi.org/10.1016/j.mex.2019.05.029, 2019.

Li, M., Zhang, T., Li, J., and Feng, P.: Hydrological Drought Forecasting Incorporating Climatic and Human-Induced Indices, WEATHER AND FORECASTING, 34, 1365–1376, https://doi.org/10.1175/WAF-D-19-0029.1, 2019.

Li, M., Feng, Z., Zhang, M., and Yao, Y.: Influence of large-scale climate indices and regional meteorological elements on drought characteristics in the Luanhe River Basin, ATMOSPHERIC RESEARCH, 300, 107219, https://doi.org/10.1016/j.atmosres.2024.107219, 2024a.

Li, X., Zhou, S., Wang, F., and Fu, L.: An improved sparrow search algorithm and CNN-BiLSTM neural network for predicting sea level height, SCIENTIFIC REPORTS, 14, 4560, https://doi.org/10.1038/s41598-024-55266-4, 2024b.

Li, Y., Li, T., and Liu, H.: Recent advances in feature selection and its applications, KNOWLEDGE AND INFORMATION SYSTEMS, 53, 551–577, https://doi.org/10.1007/s10115-017-1059-8, 2017.

Lin, Z., Ji, Y., and Sun, X.: Landslide Displacement Prediction Based on CEEMDAN Method and CNN-BiLSTM Model, SUSTAINABILITY, 15, 10071, https://doi.org/10.3390/su151310071, 2023.

Liu, Q., Huo, A., Zhao, Z., Zhao, X., Rebouh, N. Y., and Luo, C.: Spatial Differentiation and Influencing Factors Analysis of Drought Characteristics Based on the Standardized Precipitation Index: A Case Study of the Yellow River Basin, WATER, 16, 1337, https://doi.org/10.3390/w16101337, 2024a.

https://doi.org/10.5194/egusphere-2026-1033
Preprint. Discussion started: 2 April 2026

555 Liu, W., Huang, Y., and Wang, H.: Effective Deep Learning Seasonal Prediction Model for Summer
556 Drought Over China, EARTHS FUTURE, 12, e2023EF004409, https://doi.org/10.1029/2023EF004409,
557 2024b.

558 M. Schuster and K. K. Paliwal: Bidirectional recurrent neural networks, IEEE Transactions on Signal
559 Processing, 45, 2673–2681, https://doi.org/10.1109/78.650093, 1997.

560 McKee, T. B., Doesken, N. J., and Kleist, J.: THE RELATIONSHIP OF DROUGHT FREQUENCY
561 AND DURATION TO TIME SCALES, 1993.

562 Nandgude, N., Singh, T. P., Nandgude, S., and Tiwari, M.: Drought Prediction: A Comprehensive Review
563 of Different Drought Prediction Models and Adopted Technologies, SUSTAINABILITY, 15, 11684,
564 https://doi.org/10.3390/su151511684, 2023.

565 Palmer, W. C.: Meteorological drought, US Department of Commerce, Weather Bureau, 1965.

566 Prasad, R., Deo, R. C., Li, Y., and Maraseni, T.: Weekly soil moisture forecasting with multivariate
567 sequential, ensemble empirical mode decomposition and Boruta-random forest hybridizer algorithm
568 approach, CATENA, 177, 149–166, https://doi.org/10.1016/j.catena.2019.02.012, 2019.

569 Prodhan, F. A., Zhang, J., Hasan, S. S., Sharma, T. P. P., and Mohana, H. P.: A review of machine learning
570 methods for drought hazard monitoring and forecasting: Current research trends, challenges, and future
571 research directions, ENVIRONMENTAL MODELLING & SOFTWARE, 149, 105327,
572 https://doi.org/10.1016/j.envsoft.2022.105327, 2022.

573 Sayyad, S., Kumar, S., Bongale, A., Kotecha, K., Selvachandran, G., and Suganthan, P. N.: Tool wear
574 prediction using long short-term memory variants and hybrid feature selection techniques,
575 INTERNATIONAL JOURNAL OF ADVANCED MANUFACTURING TECHNOLOGY, 121, 6611–
576 6633, https://doi.org/10.1007/s00170-022-09784-y, 2022.

577 Shukla, S. and Wood, A. W.: Use of a standardized runoff index for characterizing hydrologic drought,
578 GEOPHYSICAL RESEARCH LETTERS, 35, L02405, https://doi.org/10.1029/2007GL032487, 2008.

579 Subbiah, S. S., Paramasivan, S. K., Arockiasamy, K., Senthivel, S., and Thangavel, M.: Deep Learning
580 for Wind Speed Forecasting Using Bi-LSTM with Selected Features, INTELLIGENT AUTOMATION
581 AND SOFT COMPUTING, 35, 3829–3844, https://doi.org/10.32604/iasc.2023.030480, 2023.

582 Sugihara, G., May, R., Ye, H., Hsieh, C., Deyle, E., Fogarty, M., and Munch, S.: Detecting Causality in
583 Complex Ecosystems, Science, 338, 496–500, 2012.

584 Sun, A. Y. and Scanlon, B. R.: How can Big Data and machine learning benefit environment and water
585 management: a survey of methods, applications, and future directions, ENVIRONMENTAL
586 RESEARCH LETTERS, 14, 073001, https://doi.org/10.1088/1748-9326/ab1b7d, 2019.

587 Wang, F., Lai, H., Li, Y., Feng, K., Zhang, Z., Tian, Q., Zhu, X., and Yang, H.: Dynamic variation of
588 meteorological drought and its relationships with agricultural drought across China, AGRICULTURAL
589 WATER MANAGEMENT, 261, 107301, https://doi.org/10.1016/j.agwat.2021.107301, 2022.

https://doi.org/10.5194/egusphere-2026-1033
Preprint. Discussion started: 2 April 2026

590 Wu, J., Wang, Z., Hu, Y., Tao, S., and Dong, J.: Runoff Forecasting using Convolutional Neural Networks
591 and optimized Bi-directional Long Short-term Memory, WATER RESOURCES MANAGEMENT, 37,
592 937–953, https://doi.org/10.1007/s11269-022-03414-8, 2023.

593 Wu, Z., Yin, H., He, H., and Li, Y.: Dynamic-LSTM hybrid models to improve seasonal drought
594 predictions over China, JOURNAL OF HYDROLOGY, 615, 128706,
595 https://doi.org/10.1016/j.jhydrol.2022.128706, 2022.

596 Xu, D., Zhang, Q., Ding, Y., and Zhang, D.: Application of a hybrid ARIMA-LSTM model based on the
597 SPEI for drought forecasting, ENVIRONMENTAL SCIENCE AND POLLUTION RESEARCH, 29,
598 4128–4144, https://doi.org/10.1007/s11356-021-15325-z, 2022.

599 Yalcin, S., Esit, M., and Coban, O.: A new deep learning method for meteorological drought estimation
600 based-on standard precipitation evapotranspiration index, ENGINEERING APPLICATIONS OF
601 ARTIFICIAL INTELLIGENCE, 124, 106550, https://doi.org/10.1016/j.engappai.2023.106550, 2023.

602 Yang, M., Chen, X., and Cheng, C. S.: Hydrological impacts of precipitation extremes in the Huaihe
603 River Basin, China, SPRINGERPLUS, 5, 1731, https://doi.org/10.1186/s40064-016-3429-1, 2016.

604 Zhang, R., Chen, Z.-Y., Xu, L.-J., and Ou, C.-Q.: Meteorological drought forecasting based on a
605 statistical model with machine learning techniques in Shaanxi province, China, SCIENCE OF THE
606 TOTAL ENVIRONMENT, 665, 338–346, https://doi.org/10.1016/j.scitotenv.2019.01.431, 2019.

607 Zhang, X., Hao, Z., Singh, V. P., Zhang, Y., Feng, S., Xu, Y., and Hao, F.: Drought propagation under
608 global warming: Characteristics, approaches, processes, and controlling factors, SCIENCE OF THE
609 TOTAL ENVIRONMENT, 838, 156021, https://doi.org/10.1016/j.scitotenv.2022.156021, 2022.

610 Zhou, Z., Shi, H., Fu, Q., Ding, Y., Li, T., and Liu, S.: Investigating the Propagation From Meteorological
611 to Hydrological Drought by Introducing the Nonlinear Dependence With Directed Information Transfer
612 Index, WATER RESOURCES RESEARCH, 57, e2021WR030028,
613 https://doi.org/10.1029/2021WR030028, 2021.

614 Zhou, Z., Ding, Y., Zhao, Y., Chen, P., Fu, Q., Xue, P., Liu, S., Huang, S., and Shi, H.: A new perspective
615 for assessing hydro-meteorological drought relationships at large scale based on causality analysis,
616 Environ. Res. Lett., 18, 104046, https://doi.org/10.1088/1748-9326/acfe1e, 2023.

617 Zhu, Q., Luo, Y., Zhou, D., Xu, Y.-P., Wang, G., and Tian, Y.: Drought prediction using in situ and remote
618 sensing products with SVM over the Xiang River Basin, China, NATURAL HAZARDS, 105, 2161–
619 2185, https://doi.org/10.1007/s11069-020-04394-x, 2021.

620 Zounemat-Kermani, M., Batelaan, O., Fadaee, M., and Hinkelmann, R.: Ensemble machine learning
621 paradigms in hydrology: A review, JOURNAL OF HYDROLOGY, 598, 126266,
622 https://doi.org/10.1016/j.jhydrol.2021.126266, 2021.

623